

Metallic 1T Phase, 3d¹ Electronic Configuration and Charge Density Wave Order in Molecular-Beam Epitaxy Grown Monolayer Vanadium DiteLLuride

Ping Kwan Johnny Wong,^{,1,‡} Wen Zhang,^{2,‡} Jun Zhou,² Fabio Bussolotti,³ Xinmao Yin,² Lei Zhang,^{1,2} Alpha T. N'Diaye,⁴ Simon A. Morton,⁴ Wei Chen,^{1,2,5} Johnson Goh,^{*,2,3} Michel P. de Jong,⁶ Yuan Ping Feng,^{1,2} and Andrew T. S. Wee^{*,1,2}*

¹Centre for Advanced 2D Materials (CA2DM) and Graphene Research Centre (GRC), National University of Singapore, 6 Science Drive 2, Singapore 117546, Singapore

²Department of Physics, National University of Singapore, 2 Science Drive 3, Singapore 117542, Singapore

³Institute of Materials Research and Engineering (IMRE), Agency for Science, Technology and Research (A*Star), 2 Fusionopolis Way, Innovis, Singapore 138634, Singapore

⁴Advanced Light Source (ALS), Lawrence Berkeley National Laboratory, Berkeley CA94720, USA

⁵Department of Chemistry, National University of Singapore, 2 Science Drive 3, Singapore 117542, Singapore

⁶NanoElectronics Group, MESA+ Institute for Nanotechnology, P.O. Box 217, University of Twente, 7500 AE, Enschede, The Netherlands

*E-mail: pingkwanj.wong@gmail.com; gohj@imre.a-star.edu.sg; phyweets@nus.edu.sg

Figure S1. *Ex situ* atomic force microscopy image of monolayer VTe₂.

Figure S2. Bias-dependent STM images of monolayer VTe₂.

Figure S3. ARPES constant energy map and raw intensity map of monolayer VTe₂.

Figure S4. Overlays between experimental ARPES map of monolayer VTe₂ with calculated 2H bands.

Figure S5. Se 3d XPS core-level peak of monolayer VTe₂ with pure Se as a protective cap.

Figure S6. Stoichiometric ratio and homogeneity of monolayer VTe₂.

Supplementary note 1. XMCD characterization and analysis.

Supplementary note 2. Consistent results reported elsewhere.

Figure S1. (a) *Ex situ* atomic force microscopy image showing the quasi-2D growth of monolayer VTe_2 on HOPG. Unlike monolayer VSe_2 grown with similar growth conditions,¹ the telluride film features dendrimer-like domains without sharp edges until the emergence of the second layer (highlighted with blue circles). On the other hand, the lateral size of the monolayer film is generally quite large, with a few hundreds of nanometers. Some surface adsorbates are also observed due to ambient contaminations without a Se or Se/Te cap. (b) The line profile shown in (a) shows a step height of ~ 0.8 nm, in reasonable agreement with that measured by STM (**Figure 1c** in the main text).

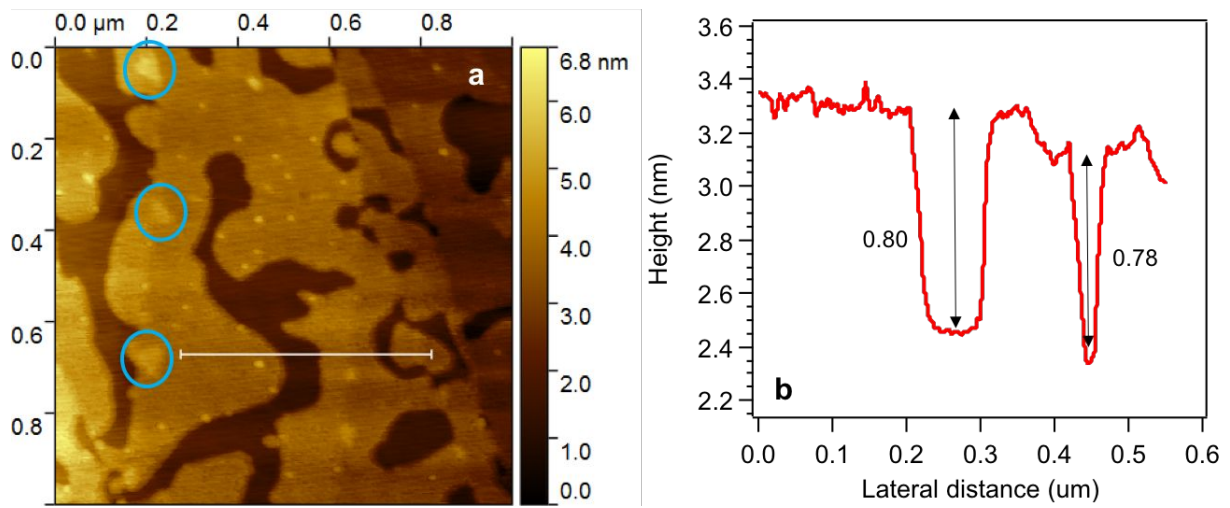


Figure S2. Bias-dependent STM images of monolayer VTe₂ highlighting the electronic effects to the topography of the captured images. With a few different tip biases (−0.5 eV, −0.08 eV, +0.2 eV), various appearances of the monolayer have been obtained. However, regardless of these variations, the (4 × 4) reconstruction due to CDW always persists. Also interesting to note is the contrast inversion in the bias-dependent STM images, which is observed as well in ref. 40. Notice that the image shown in the middle panel was not obtained from the same monolayer as the top and bottom panels, thus indicating good reproducibility of our measured results and consistency among different samples.

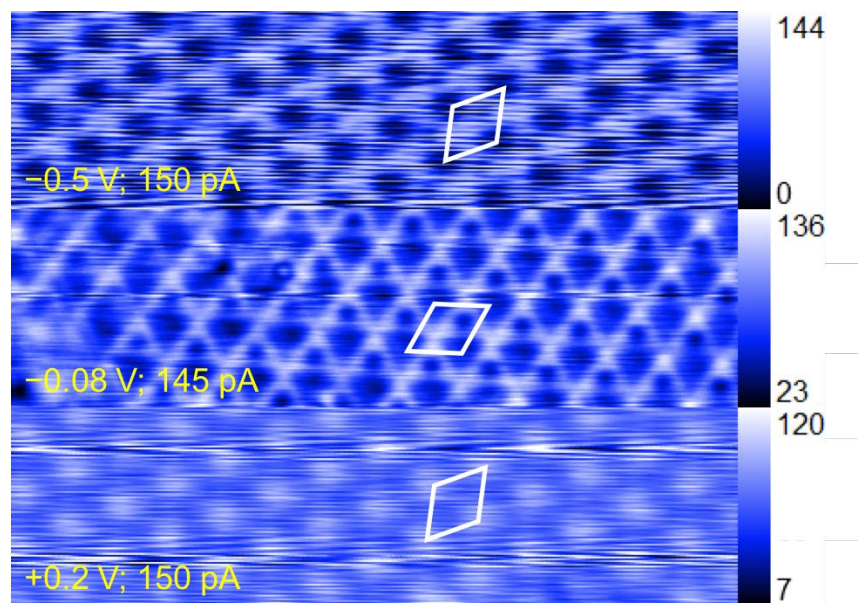


Figure S3. (a) ARPES constant energy map of monolayer VTe₂ in the 2D reciprocal space, obtained at 0.2 eV binding energy (BE). The broad circular-like intensity pattern around the Γ point represents a direct signature of the in-plane azimuthal disorder,^{2,3} in contrast with the hexagonal-like intensity modulation reported for single-oriented VTe₂ domains (see ref. 22 in the main text). (b,c) Raw intensity maps measured at 297 K and 11 K.

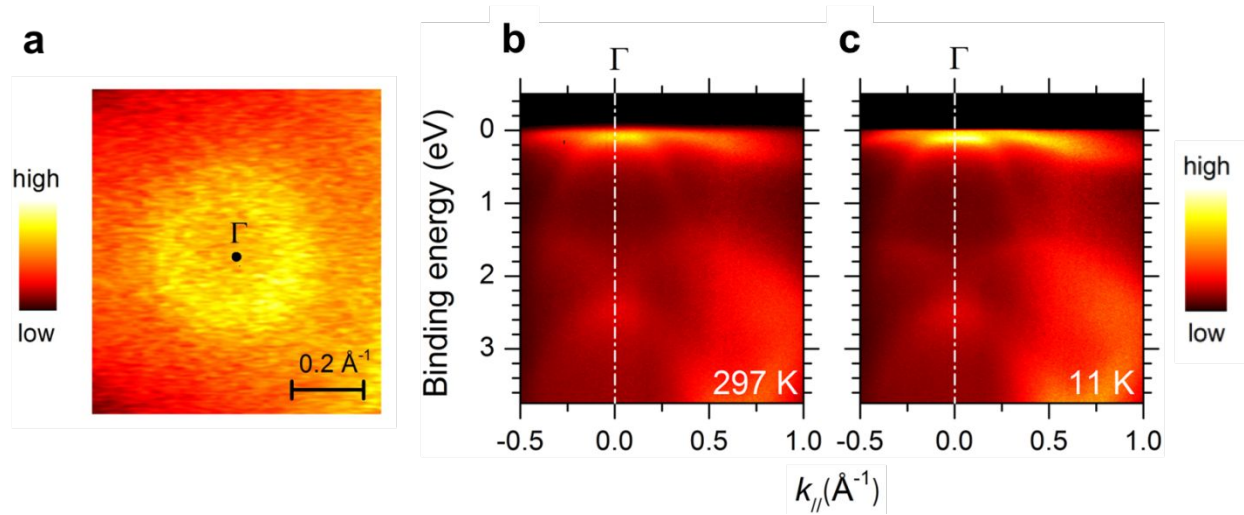


Figure S4. Overlay of the second-derivative-filtered ARPES intensity map of monolayer VTe₂ (11 K) with DFT-calculated 2H bands, which clearly indicates inconsistency between these results. Note that the dispersions along the Γ -M direction in the hexagonal Brillouin zone are in solid lines and those along the Γ -K direction in dotted lines. Zero BE represents the Fermi level position.

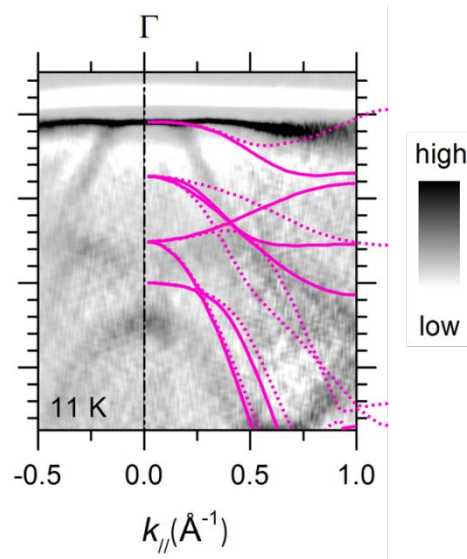


Figure S5. Se 3d XPS core-level peak of monolayer VTe₂ with pure Se as a protective cap. The measurements reveal that under various desorption conditions, non-negligible Se signals remain, indicating possible Se contamination in the monolayer film. However, it remains not known whether such Se signals are originated from Se doping in the VTe₂ lattice, besides expected absorption on the monolayer edges.

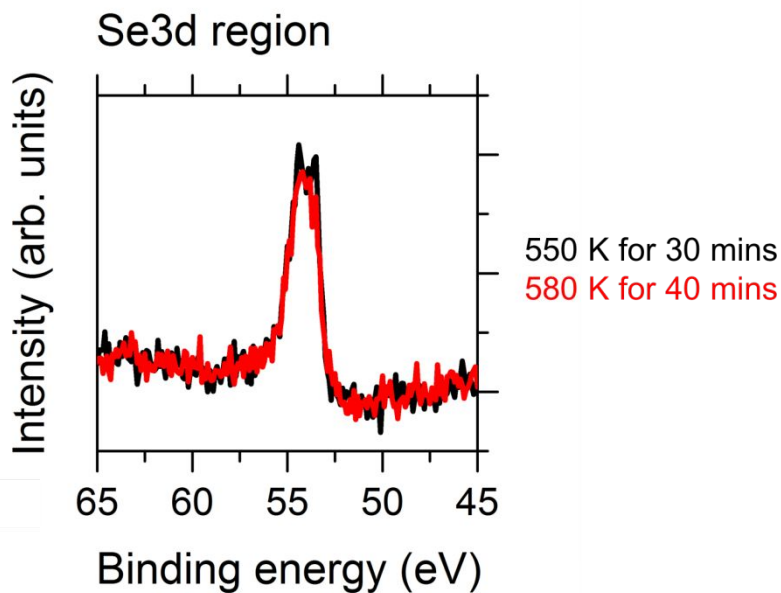
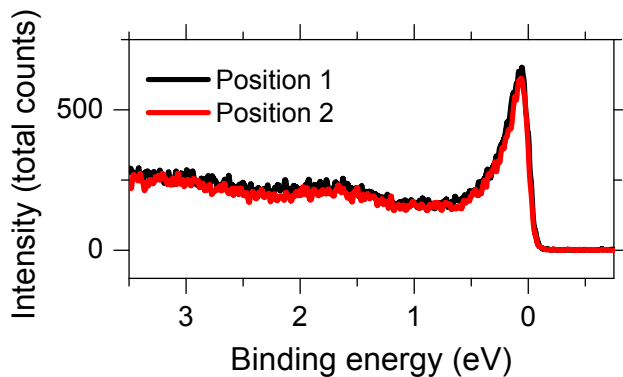


Figure S6. Energy distribution curves (EDCs) around the Γ point for different sample positions (located at ~ 1.5 mm away along z direction) over a 2×2 mm² region, probed by a beam spot of ~ 0.8 mm². No significant changes can be detected in the EDCs, thus indicating good homogeneity in the monolayer stoichiometry. We also quantified the stoichiometry from the V 2p and Te 3d XPS core-level measurements in **Figure 2a,b** (in the main text). The quantification involves integration of the core-level peak areas, followed by normalization to their respective core-level photoionization cross-sections (at 650 eV, *i.e.* the photon excitation energy used for the XPS measurements).⁴ Such analysis yields a Te/V ratio of 1.92, which is reasonably close to an ideal ratio of 2. Yet, its slight deviation from the perfect stoichiometry may be related to the presence of atomic-scale structures, such as Te vacancies, grain boundaries, edges, *etc.* Some of these are indeed evident in **Figure 1b** and similarly reported for other MBE-grown 2D-transition metal dichalcogenides, such as VSe₂, where Se vacancies have been observed.⁵ The slightly deviated stoichiometry of our monolayer might also be fundamentally originated from the small electronegativity difference between V and Te, relative to those of more electronegative S and Se, leading to the weak V-Te bonds in VTe₂. Next, to check the film homogeneity, we obtain a distribution of the Te/V ratio (1.94, 1.89, 1.95, 1.92, 1.91, 1.98) for 6 different positions over a sample size of 5×5 mm² with a probe spot of $\sim 3 \times 0.5$ mm². Using the standard formula $\sigma = \sqrt{\frac{1}{N} \sum_{i=1}^N (x_i - \mu)^2}$, we obtain a mean Te/V ratio $\mu = 1.93$, with a narrow standard deviation $\sigma = 0.029$, thus indicating a good stoichiometric homogeneity of our MBE-grown monolayer film. In particular, we note that this mean ratio is quite comparable with that reported for bulk VTe₂ crystal (Ve/T = 1.92; ref. 12 in the main text).



Supplementary note 1. XMCD characterization and analysis. In contrast to conventional magnetic measurement tools, XMCD is an advantageous tool, not only because of its element-specificity guaranteeing the observed magnetic contrast to be intrinsic to VTe_2 (this issue has previously spurred a great deal of controversy in the experimentally observed magnetism in monolayer VSe_2 , as already discussed in the manuscript), but also due to its high sensitivity for detecting weak dichroism down to one in 3×10^4 in spectroscopy, *i.e.*, 0.03% (with both optimized sample and measurement setting at the ALS beamline). This sensitivity, for V, roughly corresponds to a moment of $4\text{--}7 \times 10^{-3} \mu_{\text{B}}$, given the $\sim 7.5\%$ dichroism and $\sim 1 \mu_{\text{B}}$ per V atom in $\text{Fe}_{0.9}\text{V}_{0.1}$ alloy⁶ and the $\sim 1.8\%$ dichroism and $\sim 0.4 \mu_{\text{B}}$ per V atom in cobalt-capped monolayer VSe_2 (ref. 29 in the main text). We consider the latter as a fair reference for the present discussion, particularly because both VSe_2 and VTe_2 are in the VX_2 group, thus sharing similar structural and electronic properties, and their XMCD characterizations have also been performed across the same V- $L_{2,3}$ absorption edge. Considering the theoretical moment of $\sim 0.6 \mu_{\text{B}}$ (ref. 20 in the main text), we expect a dichroism larger than 1.8% for monolayer VTe_2 , but **Figure 4c** only indicates a value less than 0.1% (if exists). We point out that such tiny signals are probably not of a magnetic origin, because the signals did not change signs as the applied magnetic field direction was flipped. In fact, the absence of intrinsic ferromagnetism in monolayer VTe_2 as concluded from our XMCD measurements is consistent with the ARPES intensity maps in **Figure 3**, evidencing a lack of exchange-split V 3d bands. Our observation at this point is also supported by a recent work appeared after the submission of our work (**Supplementary note 2**), showing a negligible XMCD in monolayer VTe_2 similarly grown by MBE, even up to an applied magnetic field of 5 T.⁸

Supplementary note 2. During peer-review of this manuscript, we became aware of the appearance of manuscripts⁷⁻⁹ that report consistent results with our work, especially with both refs. 7 and 8 showing the (4×4) CDW in monolayer VTe₂ and ref. 9 an unresolved CDW gap manifested as a minor dip feature in STS measurements at 78 K as well as bias-dependent STM contrast inversion.

REFERENCES

1. Wong, P. K. J.; Zhang, W.; Bussolotti, F.; Yin, X.; Heng, T. S.; Zhang, L.; Huang, Y. L.; Vinai, G.; Krishnamurthi, S.; Bukhvalov, D. W.; Zheng, Y. J.; Chua, R.; N'Diaye, A. T.; Morton, S. A.; Yang, C.-Y.; Ou Yang, K.-H.; Torelli, P.; Chen, W.; Goh, K. E. J.; Ding, J. *et al.* Evidence of Spin Frustration in a Vanadium Diselenide Monolayer Magnet. *Adv. Mater.* **2019**, *31*, 1901185.
2. Zhou, S. Y.; Gweon, G. -H.; Spataru, C. D.; Graf, J.; Lee, D. -H.; Louie, S. G.; Lanzara, A. Coexistence of Sharp Quasiparticle Dispersions and Disorder Features in Graphite. *Phys. Rev. B* **2005**, *71*, 161403(R).
3. Bussolotti, F.; Chai, J. W.; Yang, M.; Kawai, H.; Zhang, Z.; Wang, S. J.; Manzano, C.; Huang, Y. L.; Chi, D. Z.; Goh, K. E. J. Electronic Properties of Atomically Thin MoS₂ Layers Grown by Physical Vapour Deposition: Band Structure and Energy Level Alignment at Layer/Substrate Interfaces. *RSC Adv.* **2018**, *8*, 7744.
4. Yeh, J. J.; Lindau, I. Atomic Subshell Photoionization Cross Sections and Asymmetry Parameters: $1 \leq Z \leq 103$. *Atomic Data and Nuclear Data Tables* **1985**, *32*, 1-155.
5. Liu, Z. -L.; Lei, B.; Zhu, Z. -L.; Tao, L.; Qi, J.; Bao, D. -L.; Wu, X.; Huang, L.; Zhang, Y. -Y.; Lin, X.; Wang, Y. L.; Du, S. X.; Pantelides, S. T.; Gao, H. -J. Spontaneous Formation of 1D Pattern in Monolayer VSe₂ with Dispersive Adsorption of Pt Atoms for HER Catalysis. *Nano Lett.* **2019**, *19*, 4897-4903.
6. Spin-Dependent X-Ray Absorption Spectroscopy of 3d Transition Metals: Systematics and Applications. PhD Thesis, Freie Universität Berlin, Deutschland, October 2003.
7. Sugawara, K.; Nakata, Y.; Fujii, K.; Nakayama, K.; Souma, S.; Takahashi, T.; Sato, T. Monolayer VTe₂: Incommensurate Fermi Surface Nesting and Suppression of Charge Density Waves. **2019**, *99*, 241404(R).
8. Coelho, P. M.; Lasek, K.; Cong, K. N.; Li, J. F.; Niu, W.; Liu, W.Q.; Oleynik, I. I.; Batzill M. Monolayer Modification of VTe₂ and Its Charge Density Wave. *J. Phys. Chem. Lett.* **2019**, *10*, 4987-4993.

9. Miao, G.; Xue, S.; Li, B.; Lin, Z.; Liu, B.; Zhu, X.; Wang, W.; Guo, J. Real-Space Investigation of the Charge Density Wave in VTe₂ Monolayer with Rotational and Mirror Symmetries Broken. **2019**, 1908.00714. *arXiv*. <https://arxiv.org/abs/1908.00714> (Aug 2, 2019).